

Scanningless depth-resolved microscopy

Dan Oron, Eran Tal and Yaron Silberberg

Department of physics of Complex Systems, The Weizmann Institute of Science, Rehovot
76100, Israel

dan.oron@weizmann.ac.il

Abstract: The ability to perform optical sectioning is one of the great advantages of laser-scanning microscopy. This introduces, however, a number of difficulties due to the scanning process, such as lower frame rates due to the serial acquisition process. Here we show that by introducing spatiotemporal pulse shaping techniques to multiphoton microscopy it is possible to obtain full-frame depth resolved imaging completely without scanning. Our method relies on temporal focusing of the illumination pulse. The pulsed excitation field is compressed as it propagates through the sample, reaching its shortest duration at the focal plane, before stretching again beyond it. This method is applied to obtain depth-resolved two-photon excitation fluorescence (TPEF) images of drosophila egg-chambers with nearly 10^5 effective pixels using a standard Ti:Sapphire laser oscillator.

© 2005 Optical Society of America

OCIS codes: (170.0110) Imaging systems; (180.2520) fluorescence microscopy; (190.4180) Multiphoton processes.

References and links

1. M. Minsky, *Microscopy apparatus*, US patent 3,013,467, Dec. 19 (1961).
2. T. Wilson, *Confocal Microscopy*, Academic press, London (1990).
3. W. Denk, J.H. Strickler, W.W. Webb, "Two-photon laser scanning fluorescence microscopy," *Science* **248**, 73 (1990).
4. C.J.R. Sheppard, X.Q. Mao, "Confocal microscopes with slit apertures," *J. Mod. Optics* **35**, 1169 (1988).
5. G.J. Brakenhoff, J. Squier, T. Norris, A.C. Bliton, M.H. Wade, B. Athey, "Real-time two-photon confocal microscopy using a femtosecond, amplified, Ti:Sapphire system," *J. Microscopy* **181**, 253 (1995).
6. M.D. Egger, Petran, "New reflected-light microscope for viewing unstained brain and ganglion cells," *Science* **157**, 305 (1967).
7. A.H. Buist, M. Muller, J. Squier, G.J. Brakenhoff, "Real-time two-photon absorption microscopy using multi-point excitation," *J. Microscopy* **192**, 217 (1998).
8. J. Bewersdorf, R. Pick, S.W. Hell, "Multifocal multiphoton microscopy," *Opt. Lett.* **23**, 655 (1998)
9. S.W. Hell, V. Andersen, "Space-multiplexed multifocal nonlinear microscopy," *J. Microscopy* **202**, 457 (2001).
10. D.N. Fittinghoff, P.W. Wiseman, J.A. Squier, "Widefield multiphoton and temporally decorrelated multifocal multiphoton microscopy," *Opt. Express* **7**, 273 (2000)
11. T. Nielsen, M. Fricke, D. Hellweg, P. Andersen, "High efficiency beam splitter for multifocal multiphoton microscopy," *J. Microscopy* **201**, 368 (2001).
12. G.J. Tearney, R.H. Webb, B.E. Bouma, "Spectrally encoded confocal microscopy," *Opt. Lett.* **23**, 1152 (1998).
13. A. Egner, S.W. Hell, "Time multiplexing and parallelization in multifocal multiphoton microscopy," *J. Opt. Soc. Am. A* **17**, 1192 (2000); V. Andersen, A. Egner, S.W. Hell, "Time-multiplexed multifocal multiphoton microscope," *Opt. Lett.* **26**, 75 (2001).
14. O.E. Martinez, "3000 times grating compressor with positive group-velocity dispersion - application to fiber compensation in 1.3-1.6 m region," *IEEE J. Quantum Electron.* **23**, 59 (1987).
15. A. Hopt, E. Neher, "Highly nonlinear photodamage in two-photon fluorescence microscopy," *Biophys. J.* **80**, 2029 (2001).
16. S.H. Cho, B.E. Bouma, E.P. Ippen, J.G. Fujimoto, "Low-repetition-rate high-peak-power Kerr-lens mode-locked Ti:Al₂O₃ laser with a multiple-pass cavity," *Opt. Lett.* **24**, 417 (1999).

17. T.B. Norris, "Femtosecond pulse amplification at 250KHz with a Ti:Sapphire regenerative amplifier and application to continuum generation," *Opt. Lett.* **17**, 1009 (1992).
18. M. Straub, S.W. Hell, "Fluorescence lifetime three-dimensional microscopy with picosecond precision using a multifocal multiphoton microscope," *Appl. Phys. Lett.* **73**, 1769 (1998).
19. S. Leveque-Fort, M.P. Fontaine-Aupart, G. Roger, P. Georges, "Fluorescence-lifetime imaging with a multifocal multiphoton microscope," *Opt. Lett.* **29**, 2884 (2004).
20. A. M. Weiner, "Femtosecond pulse shaping using spatial light modulators," *Rev. Sci. Instr.* **71**, 1929 (2000).
21. G. Peleg, A. Lewis, O. Bouevitch, L. Loew, D. Parnas, M. Linial, "Gigantic optical non-linearities from nanoparticle-enhanced molecular probes with potential for selectively imaging the structure and physiology of nanometric regions in cellular systems," *Bioimaging* **4**, 215 (1996).
22. Y. Barad, H. Eisenberg, M. Horowitz, Y. Silberberg, "Nonlinear scanning laser microscopy by third harmonic generation," *Appl. Phys. Lett.* **70**, 922 (1997).
23. M. Muller, J. Squier, K.R. Wilson, G.J. Brakenhoff, "3D-microscopy of transparent objects using third-harmonic generation," *J. Microsc.* **191**, 266 (1998).
24. M.D. Duncan, J. Reintjes, T.J., Manuccia, "Scanning coherent anti-Stokes Raman microscope," *Opt. Lett.* **7**, 350 (1982).
25. A. Zumbusch, G.R. Holtom, X.S. Xie, "Three-dimensional vibrational imaging by coherent anti-Stokes Raman scattering," *Phys. Rev. Lett.* **82**, 4142 (1999).
26. M.G.L. Gustaffson, "Surpassing the lateral resolution limit by a factor of two using structured illumination microscopy," *J. Microscopy* **198**, 82 (2000).

The confocal microscope, invented by Minsky [1] over forty years ago, revolutionized microscopy by enabling optical sectioning of microscopic samples, i.e. the rejection of out-of-focus scattering, by use of a confocal pinhole in front of the detection system. The field of confocal microscopy, which has seen tremendous advance since [2], still relies, however, on the same idea of point-by-point illumination of the sample and scanning of either the light beam or the sample in order to collect an image. The price to be paid is, of course, the time it takes to obtain a single image, which is typically limited to a few tens of milliseconds per section in current commercial systems, a limit typically set by the serial acquisition of image data points. This is an inherent limitation of the confocal method, which significantly limits its utility for fast time-resolved imaging and for reliable following of fast dynamics.

Multiphoton microscopes offer a different mechanism for optical sectioning. Rather than rejecting out-of-focus scattering, it is practically eliminated by its nonlinear dependence on the illumination intensity. A multiphoton process, most commonly TPEF, is efficient only when the peak intensity of the illuminating light is high, i.e. at the focal spot [3]. Acquisition of an image still requires, however, scanning of either the sample or the laser beam, resulting in a similar restriction of the image frame rate.

Numerous methods have been developed to increase the image acquisition rate in both confocal and multiphoton microscopes. Most involve multi-point illumination and scanning in a single spatial axis. Common examples are single-axis scanning and the use of line illumination [4, 5], or rotation of a patterned disk (in confocal microscopy) [6] or a lenslet array (in multiphoton microscopy) [7, 8, 9]. The same idea was implemented using beamsplitter arrays [10, 11] Others have used chromatic multiplexing [12]. Overall, however, image acquisition times have not been reduced significantly beyond video-rate imaging.

Performing depth-resolved microscopy completely without scanning could bring image acquisition times down to the shortest limit determined by the signal level. In a simple scanningless implementation of a multiphoton microscope the sample is illuminated with a low NA [10], but this results in a complete loss of the depth resolution property. It has been suggested that wide-field illumination maintaining the depth resolution can be done by massively splitting the excitation pulse with beamsplitter arrays, so that the generated foci overlap each other spatially but are temporally delayed relative to each other [11, 13]. Up to several tens of such time-separated foci have been generated using beamsplitter arrays, but massive splitting as required for scanningless microscopy has never been practically realized, and may result in

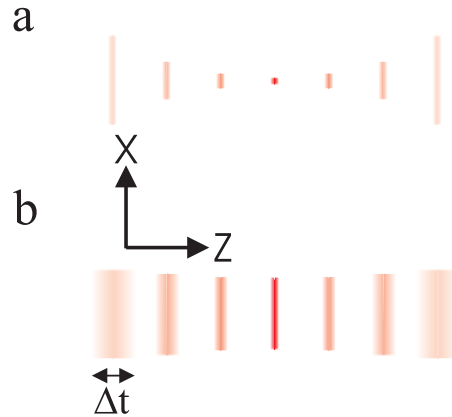


Fig. 1. (a) Cartoon of the standard multiphoton microscopy scheme: a high peak intensity at the focus of the objective lens is generated by spatial focusing of the beam, while the temporal profile of the pulse remains unchanged in passing through the sample. (b) Cartoon of the scanningless method. The beam is weakly focused, covering an area which is many orders of magnitude larger than a diffraction limited spot. A high peak intensity at the focus is achieved by modification of the temporal profile of the pulse as it propagates, reaching its peak at the focus of the objective lens.

difficulty of achieving uniform illumination for the many thousands of beamlets required to image a reasonably sized area.

In this work we suggest a different path to achieve this goal, by temporal focusing of the excitation pulse rather than by spatial focusing. This principle is demonstrated in Fig. 1. The top frame depicts the standard multiphoton technique, where an ultrashort pulse is spatially focused, generating high peak intensity at the focus; the temporal profile of the pulse (i.e. the pulse duration) remains nearly unchanged as it propagates through the sample (as the broadening due to material dispersion is negligible in microscopic samples). The lower panel is a cartoon of our new method. The illumination beam excites the full frame of interest in the specimen, an area greater by orders of magnitude than the diffraction limited spot of the objective lens. The depth resolution is achieved by controlling the temporal profile of the pulse, which is compressed as it propagates through the sample, reaching its peak value at the focal plane, and stretching again as it propagates beyond it. The depth-resolved multiphoton signal can now be collected from the entire illuminated frame using an imaging setup. Two major advantages this scheme are an inherent high illumination uniformity as it is directly related to the spatial uniformity of the excitation pulse, and scalability of the illuminated area.

The basic principle enabling these temporal manipulations can be best understood using the setup shown schematically in Fig. 2(a). It consists of a thin scattering plate, sitting at the front focal plane of a telescope. A short pulse with duration τ illuminates the plate, and each point scatters the light into many directions; each point in the image plane is also illuminated for duration τ , since all light rays emerging from a single point in the object travel identical optical pathlengths and reach the image at the same time, a concept known as the Fermat principle. However, any other point P, at some distance either from the scattering plate or from the image plane is illuminated for a longer duration, dictated by the different trajectories taken by the rays reaching it. A simple geometrical optics estimation of the illumination duration at the point P shows that the time delay of the illumination due to the two paths shown in the figure is $\Delta t = z(\cos^{-1}(\theta) - 1)/c$. The further is P from the scatterer, the longer is the illumination time. Similarly, points in front or in the back of the focal plane see extended illumination. This

principle is demonstrated in Fig. 3(a), a movie where the rays from 20 points on the scatterer are traced as they propagate to the sample. The lines represent the envelope of the ultrashort pulse (of width τc), which can be as thin as a few microns. Since any point other than the those at the focal plane is illuminated by rays emerging from different points on the scatterer, it will see an extended illumination. At the focal plane of the telescope, each point is illuminated only by rays emerging from a single point on the scatterer, resulting in an illumination of a duration of the excitation pulse itself. This way we achieve the required condition for temporal focusing.

Near the objective focal plane, the maximal pathlength difference is due to rays arriving at angles corresponding to the objective numerical aperture. Thus, it is simple to arrive at:

$$\Delta t \approx \frac{n - \sqrt{n^2 - NA^2}}{\sqrt{n^2 - NA^2}} \cdot \frac{z}{c} \quad (1)$$

where n is the refractive index and NA the numerical aperture. Equating the pulse duration τ with Δt should result in an approximate expression for the depth of the temporal focus. For high NA lenses (assuming $NA/n \approx 0.9$) this results in $z \approx \tau c/2$, corresponding to about $3\mu m$ for 20fs pulses. Taking diffraction into account does not significantly modify this geometrical optics picture. Note that this depth resolution is achieved in this case despite the fact that the entire field of view is illuminated simultaneously, in marked contrast with suggested scanningless multiphoton microscopy implementations based on temporal multiplexing of multiple foci [11, 13].

As is obvious from this description, this scheme requires very short pulses, of a duration $\tau \leq 20fs$, to achieve reasonable optical sectioning. Such pulses are typically not used for microscopy purposes, due to the increased sensitivity to dispersion and to chromatic aberrations.

In order to relax these strict requirements on the pulse duration, we note that the illuminating beam does not have to excite the entire scattering plate simultaneously. Actually, it is advantageous to tilt it, so that the illumination pulse scans across the scattering plate (and its image then scans across the object plane). The tilted geometry has the effect of reducing the depth of temporal focus since it introduces larger pathlength differences between rays arriving at any point P . This variation is illustrated in Fig. 3(b). Since the temporal focus scans across the sample just as the illumination pulse scans across the scatterer, this geometry is reminiscent of line scanning microscopy. The full frame is scanned, however, in a few picoseconds by the travelling pulse itself.

Assuming the scattering plate is illuminated at an angle α , the pulse scans across it at a velocity $v = \frac{c}{\sin(\alpha)}$. The sample is therefore scanned at a velocity $\tilde{v} = v/M$, where $M = f_1/f_2$ is the telescope magnification. When $\tilde{v} \ll c$, a geometrical optics calculation, similar to that of Eq. 1 yields $\tau(z) \propto \frac{NA}{\tilde{v}\sqrt{n^2 - NA^2}}z$. Obviously, for large magnifications this picture, leading to an arbitrarily short depth of focus regardless of the illumination pulse duration (for a sufficiently large value of M), breaks down. This limit corresponds to the case where the instantaneous illuminated area on the scatterer is imaged by the telescope onto a diffraction limited spot.

A precise analysis taking diffraction into account is analogous to the analysis of the dispersion induced by an asymmetric 4f grating compressor [14]. At the limit where the geometrical optics picture breaks down, it can be shown that the depth of temporal focus becomes identical with spatial focusing along one dimension. The criterion for achieving this optimal depth of focus for a given pulse of duration τ illuminating the scattering plate at an angle α is straightforward: that the magnification is such that the illuminated area at the scatterer is magnified by the telescope to form a diffraction limited spot, i.e.:

$$\frac{c\tau}{\sin(\alpha)} \approx \frac{M\lambda}{2NA} \quad (2)$$

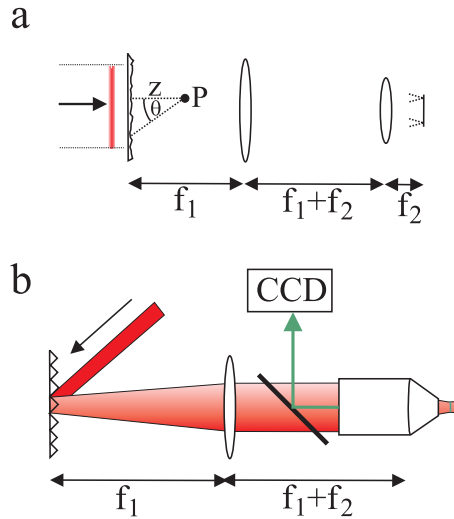


Fig. 2. (a) Principle of the scanningless TPEF microscope. A short pulse impinges upon a scatterer. At a point P further away, the pulse duration is longer due to the difference in the length of trajectories taken by the rays reaching it from different locations on the scatterer. Only at the image plane of the telescope is the pulse duration restored to its initial value, in accordance with the Fermat principle. (b) The experimental setup: The input beam impinges upon a grating, aligned perpendicular to the optic axis of the microscope. The grating is imaged through a high magnification telescope, comprised of an achromatic lens and the microscope objective, on the sample. Fluorescence is epi-detected and imaged onto a CCD using a dichroic mirror.

This is valid assuming that light is scattered from the scattering plate at large enough angles to fill the second telescope lens. In practice, for reasonable values of M , this easily enables to apply temporal focusing with pulses as long as $100f_s$. Eqs. (1) and (2) represent the two extreme regimes of temporal focusing: one where temporal focusing is achieved simultaneously over the entire sample, and is purely a geometrical optics effect. A requirement of this realization is the use of an incoherent scatterer. The other is reminiscent of line-scanning, where the sample is scanned by the travelling pulse itself. In this case temporal focusing does not depend on the coherence properties of the scatterer, and can also be achieved using a coherent scatterer.

The setup of Fig. 2(a) can be realized experimentally with a diffuser or a random phase plate serving as the scattering plate (where the required cone angle of the diffused light is determined by the requirement to fully cover the entrance aperture of the second telescope lens). This can be efficiently done provided that the undiffracted component of the illumination beam is small, a requirement which can be easily fulfilled experimentally. In contrast, the tilted illumination requires efficient off-axis scattering, which requires a blazed random phase plate. While this is impractical, an alternative realization would be the use of a coherent scatterer, i.e., a grating, for efficient off-axis scattering. Blazed gratings are an excellent candidate for use as scattering plates, due to their low cost, availability, and extremely high efficiency of off-axis scattering. It can be easily shown that fulfillment of Eq. (2) is sufficient for optimal temporal focusing in this case. Moreover, as discussed below, the coherent nature of the scattering provides additional benefits in terms of system robustness.

Figure 2(b) shows this practical setup, where a diffraction grating is used as the scattering plate. The telescope setup uses the objective as the second lens, so that fluorescence imaging can be performed in an epi-detected configuration. The field of view is determined both by the

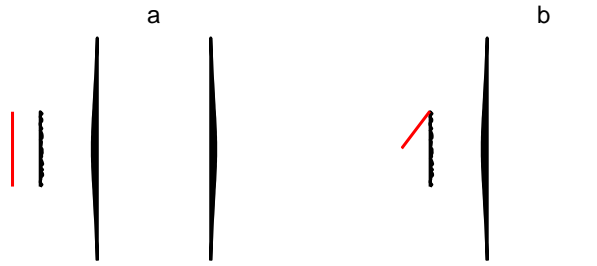


Fig. 3. Schematics movies of the temporal focusing mechanism: (a) An ultrashort pulse impinges on a scattering plate. The temporal evolution of scattered rays from 20 different points across the plate is followed (one of these wavefronts is highlighted in blue). The scattered rays denote the ultrashort pulse envelope, typically of a width of several microns. In general, points in space see an extended illumination due to pathlength difference between rays emerging from different locations on the scattering plate. Only at the image plane of the telescope all rays arriving at a point originate from a single point on the scatterer, resulting in an illumination time identical with the original pulse duration (video file of 0.72Mb). (b) Same as in (a) when the incoming pulse impinges on the scattering plate at an angle. This results in larger broadening of the pulse around the focal plane of the telescope due to the effectively increased pathlength difference. Note also the similarity of this scheme to scanning of the illumination beam in one spatial dimension, as the illumination at the focal plane occurs first at the bottom and moves towards the top (video file of 1.21Mb).

spot size on the grating and by the magnification of the telescope. While the main advantage of using a grating is that it can be designed to maximize the diffraction towards the microscope optical axis, another advantage of using a coherent scatterer is a significantly reduced sensitivity to dispersion. In a conventional multiphoton microscope the effect of dispersion is a reduction in signal intensity. In the temporal focusing scheme using an incoherent scatterer described above, it would also result in a degraded depth of focus due to the increase in pulse duration. Since the temporal focusing microscope using a grating is essentially an extremely asymmetric pulse compressor, the only effect of second order dispersion is an effective shift in the focal length of the entire system, i.e., the plane at which temporal focusing occurs will not coincide with the spatial focal plane of the objective lens. The deterioration in both the depth of the temporal focus and in the signal intensity is, in this case, only a second order effect. This peculiar property stands in great contrast to both standard and time-multiplexed multiphoton microscopes [11, 13]. In fact, modification of the second-order dispersion of excitation pulse can be used to shift the illumination plane parallel to the microscope axis. For example, rapid modulation of the excitation pulse from negative to positive second order dispersion by means of an external pulse compressor can be used to perform 3D scanning within the sample without moving either the sample or the objective lens, with possible applications such as simultaneous three-dimensional tracking of multiple particles.

Our experimental system, schematically plotted in Fig. 2(b), consists of a Ti:Sapphire laser oscillator delivering 10fs pulses at a repetition rate of 75MHz. Pulses were spatially expanded by an achromatic X3 telescope to a Gaussian shape with a diameter of 1.2cm, and directed at a 300 l/mm grating aligned perpendicular to the microscope optical axis. The illumination angle is chosen as such that the first order diffraction at the center frequency of the excitation pulse is along the optical axis of microscope. As described in the scattering plate example, the grating line density is chosen so that the pulse spectrum spans the entrance aperture of the objective lens, depending on both the magnification of the telescope and the pulse bandwidth. In our case, the telescope consisted of a 20cm achromatic lens and an X100 NA=1.4 fluar

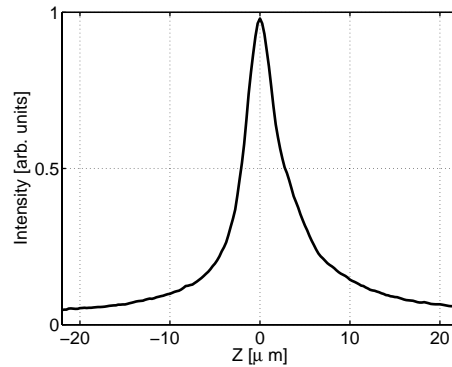


Fig. 4. Depth resolution of the scanningless TPEF microscope. The total fluorescence intensity measured from a $0.9\mu\text{m}$ thick spin-coated fluorescent layer as a function of its distance from the focal plane of the objective. Fluorescence from an area of $10^4\mu\text{m}^2$ was collected and measured with a photomultiplier tube. A CCD image of the illuminated area was used in the following to normalize for signal intensity due to the Gaussian shape of the excitation pulse.

objective (Zeiss), corresponding to a magnification of 125. This setup produced a field of view of about $100\mu\text{m}$ in diameter in the object plane. The total illumination energy per pulse was 0.4nJ , corresponding to an energy per pixel of the order of 0.01pJ (this is about two orders of magnitude below a stringent assessment of the damage thresholds [15]). The illumination uniformity is directly related to the spatial uniformity of the excitation beam. Normalizing the illumination intensity by a single 2D gaussian results in RMS nonuniformity of less than 10% over the entire field of view. As an imaging platform we use a Zeiss axiovert inverted microscope. Epi-detected fluorescence is either measured by a photomultiplier tube or imaged onto a cooled intensified CCD via a dichroic mirror and a filter which reject the excitation light. In order to avoid dispersion precompensation, the distance between the grating and the objective lens was slightly increased from $2f_1+f_2$. In this manner we compensate for both the chromatic aberration of the objective lens and the dispersion in the lenses, so as to induce TPEF at the visible focal plane of the objective. This ensures maximal transverse resolution at a cost of a slight decrease in the depth resolution.

We first demonstrate this principle by measuring the total fluorescence signal obtained from a $0.9\mu\text{m}$ layer of a two-photon fluorescent dye (Coumarin 515) in a polymer matrix spin-coated on a glass slide, as a function of its position relative to the objective focal plane. The result of such a scan is plotted in Fig. 4. The measured FWHM is $4.5\mu\text{m}$, a result comparable to that obtained for line scanning TPEF microscopy without the use of a confocal slit [5]. The asymmetry in the depth response is due to the small shift of the grating position from the focal point of the first telescope lens, as described above, and results in some deterioration of the depth resolution. Note also that due to the extremely large bandwidth of the excitation pulse, chromatic aberrations induce some smearing of the focal depth curve (of the order of $1\mu\text{m}$). Additional smearing may be due to a small tilt of the sample relative to the microscope optical axis for such a large illuminated area ($\approx 100\mu\text{m}$ in diameter).

In the imaging experiments we observed drosophila egg chambers at an early developmental stage, stained with DAPI, a fluorescent groove-binding probe for DNA, whose absorption band is centered at 400nm . Figure 5 shows eight optical cross-sections, separated by $5\mu\text{m}$. The lateral resolution of the images, determined by the numerical aperture of the objective, is $0.25\mu\text{m}$. The total area covered is $10^4\mu\text{m}^2$, corresponding to about 100,000 effective pixels. The bottom left

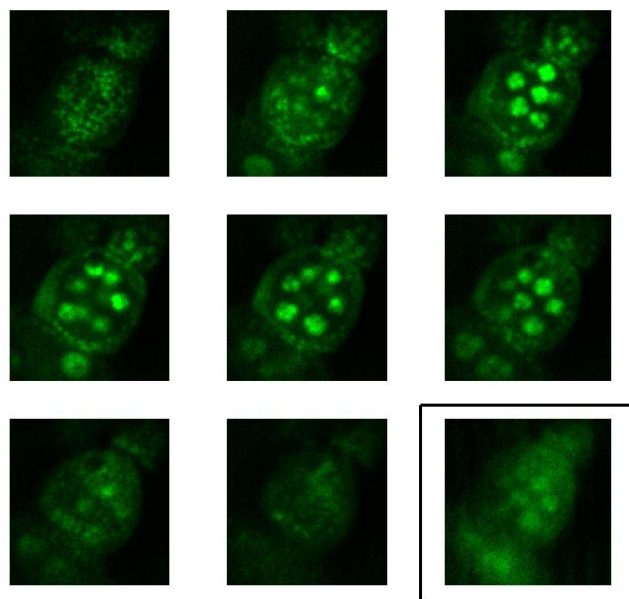


Fig. 5. Scanningless depth-resolved images of a drosophila egg-chamber stained with DAPI, a fluorescent DNA binding probe. Optical sections of a drosophila egg-chamber containing 15 nurse cells, a single oocyte and wrapped by a layer of follicle cells are presented. The images go from the bottom of the egg chamber (top left image) to its top (bottom center image). The area of each image is $140 \times 140 \mu\text{m}$. Images are separated by $5 \mu\text{m}$. The integration time for each image was 30 seconds. The intensifier noise was subtracted from each image, and it was corrected for spatial variations in the beam intensity assuming a Gaussian beam profile. On both the bottom and top sections, follicle cells, whose nuclei are approximately $3 \mu\text{m}$ in diameter, are observed. The center images show the nuclei of nurse cells, whose size is of the order of $10 \mu\text{m}$, as well as the enveloping follicle cells. A smaller egg-chamber is observed on the top right corner of the images. The bottom right image shows, for comparison, a TPEF image where the grating was replaced by a standard mirror, resulting in a non-depth resolved image. This image is to be compared with the one directly above it. While some detail can be seen, the entire egg-chamber shows a strong out-of-focus background.

image is one taken with the grating replaced by a simple mirror; hence the pulse remains short everywhere. This results in a non-depth resolved image, to be compared with the one directly above it. Significant out-of focus is observed throughout the egg-chamber.

Note that the laser system used in our experiments is far from optimal for this application, resulting in excessively long image acquisition times. A short discussion of the properties of an "ideal" system follows. In general, to optimize the nonlinear effect, short pulses are advantageous. Too short pulses ($< 20 \text{fs}$), however, should be avoided since they suffer from significant material dispersion and since their bandwidth may exceed the TPEF absorption linewidth. Long pulses ($> 100 \text{fs}$) increase complexity since large magnifications and a highly dispersive grating are required. In order to measure a maximal signal, the peak intensity at the focal plane should be as high as possible, yet remain below the damage threshold of biological specimen [5]. Lower repetition rate systems such as extended cavity lasers (operating at a few MHz)

[16] or high repetition rate amplifiers (Typically operating at a few hundred KHz) [17] are well suited to work in this regime. Extrapolating from the experiments described above, using an extended cavity 30fs oscillator, delivering $\sim 50nJ$ pulses at 10MHz (a commercially available system), video-rate scanningless full frame TPEF microscopy can be easily achieved. Working close to the damage threshold, photon rates per pixel using our scanningless scheme would be lower than those using single-point scanning only by the factor of the repetition rate reduction.

Depth-resolved microscopy has been, for decades, practically synonymous with laser-scanning microscopy. Here we showed that full-frame depth-resolved microscopy is possible, using an extremely simple setup and standard components. This opens up a range of new applications both in imaging and in time-resolved studies. For example, a scanningless setup can enable full-frame video-rate fluorescence lifetime imaging, which is less prone to artifacts due to motion on a millisecond time scale, by gating the CCD intensifier [18, 19]. Single-shot depth resolved microscopy would be able to capture extremely rapid dynamics, up to the nanosecond regime. This could be realized by using standard pulse shaping techniques [20] to split a very strong excitation pulse into a long train of pulses, each with an energy corresponding to the multiphoton damage threshold of the sample (and whose temporal spacing would be determined by the need to avoid thermal damage).

Temporal focusing is not unique to TPEF microscopy but can be used with practically any multiphoton process, such as second-harmonic generation [21], third-harmonic generation [22, 23] or coherent anti-Stokes Raman scattering [24, 25]. For these coherent imaging processes, Single-shot depth resolved microscopy could be realized by the use of a heterodyning field for increased sensitivity. The scanningless setup also enables to utilize linear optical techniques, such as structured illumination microscopy [26], leading to enhanced spatial resolution, in multiphoton imaging applications. We believe this powerful method will have a significant impact on the entire field of high-end imaging applications.

Acknowledgments

The authors would like to thank Dr. Shira Silberberg for her help with the drosophila samples.